Nonlinear fatigue crack propagation in a baffle module of Wendelstein 7-X under cyclic bending loads

Marcello Lepore[1] | Filippo Berto[2] | Angelo R. Maligno[3] | Joris Fellinger[4]

[1] Department of Industrial Engineering, University of Salerno, Via G. Paolo II 132, 84084 Fisciano, (SA), Italy

[2] Department of Mechanical and Industrial Engineering, NTNU, Richard Birkelands vei 2b, 7491 Trondheim, Norway

[3] Institute for Innovation in Sustainable Engineering, University of Derby, Derby, UK

[4] Max-Planck-Institute of Plasma Physics, Wendelsteinstraße 1, Greifswald 17491, Germany

Correspondence

Marcello Lepore, Department of Industrial Engineering, University of Salerno, Via G. Paolo II 132, 84084 Fisciano (SA), Italy. Email: malepore@unisa.it

Abstract

Simulation of the fatigue crack propagation in a Wendelstein 7-X baffle module is performed in this study using both a finite element method-based software and the UniGrow nonlinear model for small-scale yielding (SSY) conditions. Some experimental fatigue tests of several cracked baffle modules have been performed through a servo-hydraulic machine. One of these experimental tests has been considered to simulate fatigue crack propagation in the baffle module. Before starting the experimental test, a first crack partly contained in the welding seam and partly in the steel pipe is found. Subsequently, owing to the applied load, the crack propagated both into the welding seam and into the steel pipe until the plastic zone in the near field attains SSY conditions. Finally, owing to the increase in the extension of the plastic zone, SSY conditions are not more valid, and the breakage of the steel pipe is produced by plastic collapse.

KEYWORDS

cyclic bending, fatigue crack growth, SSY, UniGrow, Wendelstein 7-X

1 | INTRODUCTION

Linear elastic fracture mechanics (LEFM) is based on the small-scale yielding (SSY) hypothesis in the near field. In LEFM, numerical analyses performed using the finite element method (FEM) or dual boundary element method (DBEM) do not consider plastic zone extension and the crack length corrective term introduced by Irwin or Dugdale, namely, the effective crack length (a_{eff}).

In ductile materials, stable crack growth is associated with yielding that occurs in a small region immediately ahead of the crack front. This region is called the "plastic zone." Generally, the stable crack growth process is controlled by the local stress and strain fields within the

plastic zone where a high damage accumulation occurs. Thus, a relatively large plastic area affects the propagation life of the component, ie, extending or reducing its life.

When the yielding area in the vicinity of the crack front is extended such that LEFM cannot correctly describe the stress-strain field ahead of the crack front, the SSY conditions must be considered. Brocks defined SSY conditions as an extension of LEFM,[5] while Newmann,[18] Kuna,[20] and Zhender[33] defined SSY conditions within the elastic plastic fracture mechanics (EPFM). According to these authors, EPFM can be divided into SSY and large-scale yielding (LSY). It is noteworthy that modelling the crack using an FEM-based approach in SSY permits to stay that the relation $J = K^2/E$ is still valid, namely the stress-strain field near the crack front still depends on the elastic material behaviour surrounding the crack. In the literature and for SSY conditions, several models for fatigue crack propagation exist; however, only a few of these can be introduced in commercial codes for fracture mechanics such as Zencrack[34] or Franc3D.[14] Among the latest models, the UniGrow model for fatigue crack propagation[25] can provide a good approximation of the propagation life of a structural component. Similar to Kujawski-Ellyin's model,[19] UniGrow is a two-scale model because it considers both microstructural and macrostructural damages that occur within the plastic zone. Nevertheless, before executing a numerical simulation, plasticity must be activated, and nonlinear material properties must be modelled. Furthermore, the absence of volume forces and stress-free crack surfaces must be considered to prevent J-integral path-dependence.[5]

By employing the deformation theory of plasticity and introducing the "path-independent integral" by Cherepanov[6] and Rice,[31] a perfect analogy to LEFM can be established in EPFM. The J-integral is subsequently referred as an intensity parameter of the crack-tip fields as well as a plastic energy release rate.[5] The determination of J-integral in FE codes is based on the domain integral method in contour integral evaluation, which was first suggested by Parks[27,28] and further improved by DeLorenzi.[10,11] This method has been proven to be robust, and accurate values are obtained even by employing relatively coarse meshes.[24] As the domain integral is based on energy quantities and is over a finite region of elements, discontinuities of stresses or any other numerical imprecisions of local field quantities do not cause significant deviations.[5] Furthermore, the J-integral is defined in terms of the energy release rate associated with a fictitious advancing small crack. Because of this interpretation, the domain integral method is also known as the "virtual crack extension" (VCE) method.[5]

To calculate the size of the plastic zone, an effective crack length, a_{eff}, is obtained corresponding to an effective stress intensity factor (SIF), K_{eff}. In these conditions, an effective energy release rate[5] for SSY conditions can be written as $G_{SSY} \approx G_e + G_p$, where G_e and G_p are the elastic and plastic terms of ERR, respectively.[5]

The SIF range, ΔK expressed by models proposed for SSY conditions, is equivalent to an elastic plastic term obtained by the conversion of the effective ERR, $\Delta\sqrt{G}$, via a conversion factor (f_{conv}).[23]

Currently, Wendelstein 7-X (W7-X) is the world's largest modular stellarator to conduct nuclear fusion experiments at the Max Plank Institute (Greifswald, Germany). A hydrogen plasma is generated inside a plasma vessel (PV), and extremely high heat fluxes are radiated on the first wall of the plasma facing components.[7-9,32] The associated baffles and heat shields are both made of graphite tiles that are bolted with low pre-stress onto a heat sink of CuCrZr.[7-9,32] The heat sink was brazed onto a water-cooled steel pipe of 12-mm outer diameter and 1-mm thickness. The baffles are needed to cool the PV under operative conditions, and they were supported rigidly on a steel structure while the heat shields were connected flexibly with pins onto the PV wall.

The heat sinks were brazed onto the steel pipes that were subsequently bent and twisted into the desired shapes to replicate the complex three-dimensional internal shape of the W7-X PV. This process was performed on a bending machine in which the force was transferred from the machine via the heat sinks onto the pipes (Figure 5). A soon as the one of the brazed samples experienced the onset of cracks during bending, all baffles and heat shields were inspected to assess the presence of cracks.

It was found that 144 cracks had developed in the root of the braze in 31 different locations. None of the cracks directly caused a loss of leak tightness; however, it was feared that these first cracks might jeopardise the fatigue life of the baffles and heat shields.

It is important to notice that baffles are supported more rigidly than the heat shields; thus, they are subjected to the highest mechanical stresses during the operations of the machine. Therefore, it is paramount to implement, accurately, damage tolerance assessment tools in order to avoid a costly remanufacturing and even redesign processes of the components.

2 | MATERIALS AND METHODS

To model the AISI 316L steel hardening of the pipe, a bilinear kinematic hardening model was adopted while

the CuCrZr (heat sink) and brazing material behaviour were modelled assuming pure linear kinematic hardening.[13] For a hardening material, the material law can be modelled both in the known form of the Ramberg-Osgood equation or in the form of a linear piecewise, but only for SSY conditions. However, although using a linear piecewise material law introduces a discontinuity in the slope (J path-dependence), the contour integral method can accurately assess the J-integral solution in SSY conditions. The brazing and heat sink material properties have been considered for modelling the structural components; however, they have not been reported herein for brevity and because they are already available in the literature.[13,15] The pipe steel was modelled using the properties obtained by tensile tests performed in-house, coupled with a bilinear kinematic hardening model. In Figure 1, the material properties of the AISI 316L (Table 1) and the Ramberg-Osgood stress-strain curve are shown.

It is interesting to notice that that in this case, the strain hardening exponent, n, has been calculated to be 6.02.

As n is less than 10, no ideal plasticity occurs.[20] For assessing the microstructural damage that occurs within the plastic zone, low cycle fatigue (LCF) properties must be considered. Such properties for the AISI 316L (Table 2) have been considered in the literature[15,29] and have been introduced in the UniGrow law for fatigue crack propagation through a special FORTRAN routine within Zencrack.[34]

Macro damage is related to the yielding that occurs in the plastic zone. In the UniGrow model, yielding increases or decreases as the plastic zone (fracture process
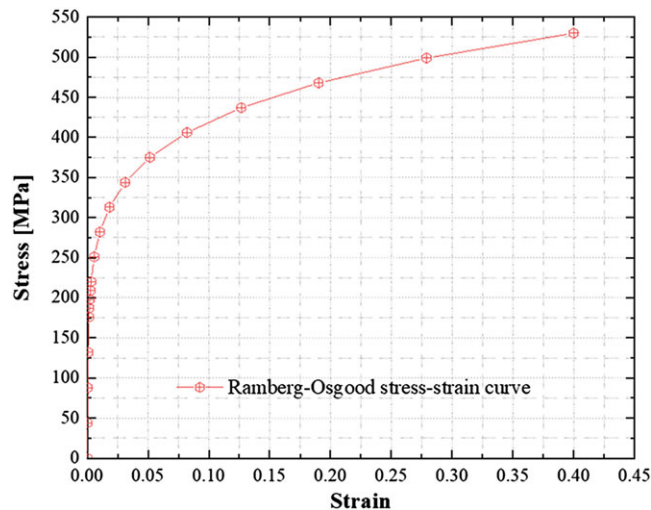
TABLE 1 Material properties of AISI 316L

E (Young's Modulus)	σ_{ys} (Yield Strength)	σ_u (Ultimate Strength)	ε_{max} (Strain at Rupture)
200 000 N/mm^2	220 N/mm^2	530 N/mm^2	40%

TABLE 2 Threshold of ΔK and LCF properties for AISI 316L

ΔK_{th} (MPa$\sqrt{mm}$)	σ'_f (MPa)	ϵ'_f	n'	b	c
149	565	1.738	0.148	−0.085	−0.575

zone) decreases or increases, respectively. Thus, vigilance is required when establishing the extension of the plastic zone to obtain an accurate estimation of propagation life for the structural component.
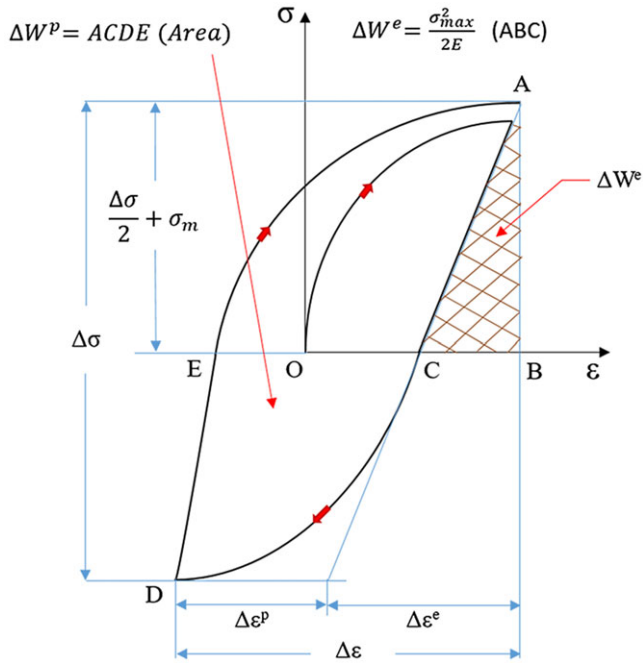
The UniGrow model only depends on $\Delta\sigma$ and σ_m, ie, the local mean stress. Hence, the UniGrow is a nonlinear law for fatigue crack growth prediction. The term $\Psi_{y,1}$, included in the UniGrow formulation, represents the averaging constant corresponding to the i-th elementary block (constant) as described in some recent works[25,26] and is equal to 1.633.

Where, b is the fatigue strength exponent; c is the fatigue ductility exponent; σ'_f is the fatigue strength coefficient, and ϵ'_f is the fatigue ductility coefficient; n′ is the cyclic strain hardening exponent, and K′ is the cyclic strength coefficient; and R is stress ratio ($R = 0.1$). The length, ρ^*, is the fracture process zone, namely the Dugdale's effective crack length based on the Edmund and Willis formulation.[12]

In SSY conditions, the elastic strain energy density is much lower than the plastic strain energy density. In Figure 2, the elastic and plastic strain energy densities for a uniaxial cyclic loading are shown for a hardening material.

Initial crack is introduced at the selected locations of the specimen, in an uncracked FEM model using the constrained crack faces technique (CCFT).[21,23] Such a defect cannot be considered as a "crack" because of the enforcement of material continuity by the application of contact constraints that prevent interpenetration, as well as the mutual displacement of the crack faces. Hence, the "cracked" FE model is equivalent to the uncracked model.[21,23]

During the simulation of the fatigue crack propagation, the contact constraints imposed on the crack faces must be removed to allow for the residual stresses to redistribute, thus resulting in a new equilibrium condition. In nonlinear elastic fracture mechanics, the

FIGURE 1 Ramberg-Osgood stress-strain curve for AISI 316L [Colour figure can be viewed at wileyonlinelibrary.com]

FIGURE 2 Elastic and plastic strain energy density for uniaxial cyclic loading case, for a hardening material and Masing behaviour [Colour figure can be viewed at wileyonlinelibrary.com]

Hutchinson Rice Rosengren singularity would be considered[16]; however, special crack-tip elements for modelling this singularity have not been established yet. In the adopted tool for fracture mechanics, Zencrack, "retained" tip elements are available. They are similar to the collapsed elements but with an unchanged mid-side node (20-node hexahedral element). Considering a hexahedral eight-node element, a mid-side dummy node is set automatically by the Zencrack code, such that an ideal plastic of singularity $1/r$ in the strains is obtained.[20]

2.1 | Geometry, loads, and boundary conditions

The geometric model of the baffle module specimen is shown in Figure 3. A straight pipe welded to the heat sinks by brazing is shown in the configuration preceding the plastic deformation of specimen N. 6078 (Table 3). Subsequently, bending is simulated by an elastic plastic FEM analysis until the final angle of 168° is reproduced. At the end of this phase, the residual stresses owing to such preliminary pipe deformation are available for the next load steps.

Three loading steps are studied to replicate the experimental analyses (Figure 4):

- *pipe pre-bending*: the straight pipe is bent by rotating the reference point RP_2 of 12° (RP_2 displacement
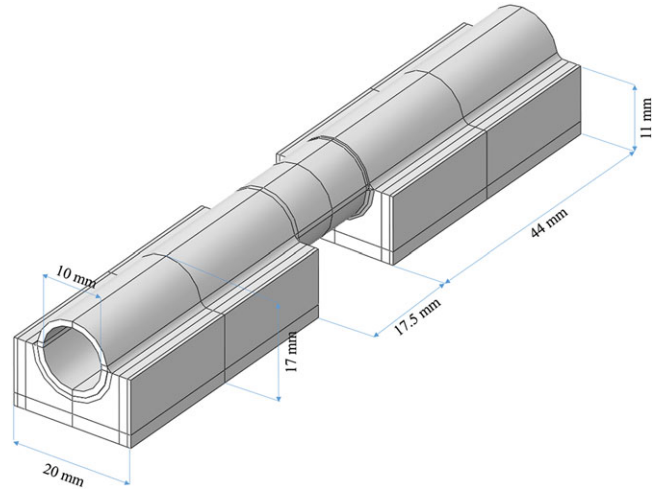
FIGURE 3 Model geometry of the specimen highlighting the boundary and loading conditions [Colour figure can be viewed at wileyonlinelibrary.com]

along the local Z-axis is allowed) while RP_1 remained clamped. The crack is already inserted, but the crack face opening is not allowed in this step by means of the CCFT[21,23];

- *load releasing*: RP_2 is released, and the final configuration with an angle of 12° representative of the specimen N. 6078 deformation is achieved at the end of this step. The crack is allowed to open between steps 1 and 2 by removing crack faces constraints previously imposed;

- *bending load application*: a bending load is applied in the -X local direction at the RP_1 (perpendicular to the related CuCrZr plate). In addition, a spring acts in the Z local direction (along the pipe axis) at RP_1. The bottom surface of the CuCrZr plate below RP_1 is maintained clamped.

Reproducing the experimental pipe bending test, the initial crack is inserted into the braze root modelled between the pipe and the heat sink. Such a crack is maintained closed using the CCFT during step 1[21,23]; the opening of the crack faces is enabled only at the end of step 1. The crack is modelled to be comparable to one of the real cracks measured by computer tomography (CT) scan on the affected components. The geometry of initial crack can already be found in the literature.[13]

In RP_1, the applied load was 1000 N, while the rotation along the Y-axis and the displacement along the Z-axis were free. Furthermore, in RP_1, a calibrated spring of stiffness 17 905 N/mm was applied along the Z-direction.

TABLE 3 Tested specimens

CT Number	Probe	Braze Seam	Imposed Bending, °	Imposed Torsion, °	Type of Initial Crack	Type of Test
6091	P5	1i	12	4	Crack over whole perimeter up to and into the steel pipe	Static
6090	P5	2i	10	5	Crack over whole perimeter up to but not into the steel pipe	Static
6075	P1	2i	17	0	Multiple crack along perimeter seam	Fatigue
6078	**P3**	**1i**	**12**	**0**	**Small crack along perimeter seam**	**Fatigue**
6087	P4	2i	12	7	Crack over whole perimeter up to and into the steel pipe	Fatigue
6093	P6	2a	16	4	Crack over whole perimeter up to and clearly into the steel pipe	Fatigue
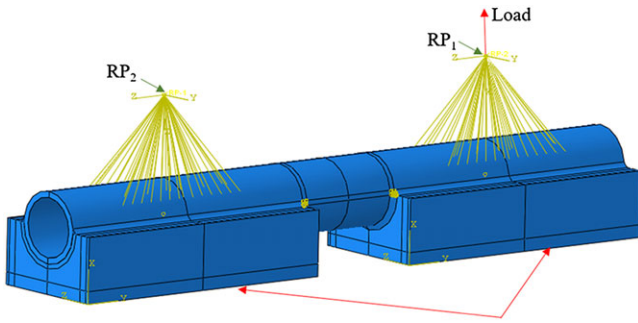
FIGURE 4 Two distributed couplings are adopted to constrain the displacements of two CuCrZr heat sinks: All the DOFs of the CuCrZr bottom surfaces are connected directly to the reference points RP$_1$ and RP$_2$ (green arrow) [Colour figure can be viewed at wileyonlinelibrary.com]

2.2 | Propagation law

The unified two-parameter fatigue crack growth driving force model (UniGrow)[25] considers the residual stress owing to the application of a cycle load and, subsequently, the stress ratio effect on the fatigue crack growth. The driving force, $\Delta\kappa$, is expressed as a combination of the maximum SIF, K_{max}, and the SIF range, ΔK, corrected for the residual stresses. In its more general formulation that considers the mean stress or the stress ratio effect on fatigue crack propagation, the deformation at the crack-tip material is considered as predominantly plastic. However, for the simulation of this study case, the adopted driving force formulation is described considering nonlinear material behaviour and is subject to cyclic loading. Subsequently, the UniGrow model is written with some modifications within a FORTRAN routine and subsequently passed to Zencrack during the simulation, similar to the previous nonlinear case. Hence, two primary difficulties arise with this approach: the first is related to the determination of $K_{max,tot}$ and ΔK_{tot}, which requires substantial fatigue data[26]; the second is related to the determination of the elementary particle of a finite

dimension, ρ^*, ie, of the process zone length.[26] To solve the former problem, the solution provided by Huffman was adopted.[17] Hence, $K_{max,tot}$ and ΔK_{tot} are calculated with Equation 1 that, for positive stress ratio, can consider residual stresses:

$$K_{max,tot} = K_{max}\left\{1 - \left[\frac{(\sigma_{\varepsilon p=0.05} - \sigma_{ys})}{\sigma_{\varepsilon p=0.05}}\right](1 - R)\right\} \quad (1)$$

where $\sigma_{\varepsilon p = 0.05}$ is the stress at 0.05 plastic strain, σ_{ys} is the yield strength, and $R = 0.1$ is the stress ratio imposed with a remote load. It is noteworthy that the K_{max} introduced in the UniGrow model originates from the Zencrack calculation of the ERR and is subsequently converted to K_{max} using the known R-ratio. In other words, in SSY conditions, a conversion factor, f_{conv}, expressed with Equation 2 must be used for calculating ΔK from the ERR, expressed in term of $\Delta\sqrt{J}$. Thus,

$$f_{conv} = \sqrt{E/(1 - \alpha v^2)} \quad (2)$$

where α is a term to describe the plane stress or plane strain condition.[34]

The resulting equation is as follows:

$$\Delta K = \Delta\sqrt{J} f_{conv.} \quad (3)$$

Subsequently, $K_{max,tot}$ is calculated using Equation 1, and $K_{min,tot} = K_{min}$ because the minimum SIF is unaffected by the residual stresses and is thus equal to the applied K_{min}. Therefore, ΔK_{tot} is calculated using $K_{max,tot}$ and K_{min}. Subsequently, starting from the Paris law, the UniGrow model can be written as follows:

$$da/dN = C (\Delta\kappa)^\gamma \quad (4)$$

where

$$\Delta\kappa = \left(K_{max,tot}^p \, \Delta K_{tot}^{0.5}\right) \quad (5)$$

and $\gamma = -1/b$. $\quad (6)$

Further, $C = 2\rho^* \left\{ \dfrac{1}{2\left(\sigma'_f\right)^2} \left[\left(\dfrac{\psi_{y,1}}{\sqrt{2\pi\rho^*}}\right)^{3n'+1} \left(\dfrac{K'}{E^{n'}}\right) \right]^{\frac{1}{n'+1}} \right\}^{\frac{-1}{2b}}$

(7)

with $= \dfrac{n'}{(n'+1)}$, and $K' = \dfrac{\sigma'_f}{\left(\epsilon'_f\right)^{n'}}$ is the cyclic strength coefficient, obtained analytically.

Subsequently, the crack growth rate can be expressed in the following form:

$$\frac{da}{dN} = 2\rho^* \left\{ \frac{1}{2\left(\sigma'_f\right)^2} \left[\left(\frac{\psi_{y,1}}{\sqrt{2\pi\rho^*}}\right)^{3n'+1} \left(\frac{K'}{E^{n'}}\right) \right]^{\frac{1}{(n'+1)}} \right\}^{\frac{-1}{2b}} \left(K^p_{max,tot}\, \Delta K^{0.5}_{tot}\right)^{\gamma}$$

(8)

where ρ^* can be used with the following formula:

$$\rho^* = r_c = \frac{\pi}{24} \left(\Delta K_{tot} / \sigma_{ys}\right)^2.$$

(9)

Subsequently, r_c is the radius of the cyclic plastic zone, σ_{ys} is the yield strength of the material, and ΔK_{tot} is obtained as the difference between $K_{max,tot}$ and K_{min} as previously described. Equation 9 resembles the plastic zone size correction proposed by Edmunds and Willis[12] in which, instead of K_I, ΔK_{tot} is used. However, it is worth noting that for notched components, similar values of r_c also are proposed in the literature.[2,3,30] Moreover, in Equation 9, σ_{ys} is used instead of σ_{yc} because ΔK_{tot} in the modified version of UniGrow model (1) is expressed as function of R-ratio that depends on the monotonic load. Finally, it is noteworthy that the fatigue crack propagation law (8) is written using the Manson-Coffin equation, in which the plastic term is omitted.[26] Additionally, it should be noted that the driving force (5) results directly from the mean stress correction model, ie, the Smith, Watson, and Topper fatigue damage parameter.[26]

3 | RESULTS AND DISCUSSION

3.1 | Experimental pipe bending

Various types of cracks are created in the specimens owing to the imposed bending and torsion to obtain the desired shapes (Table 3). All the cracks are positioned at the external surface of the braze roots. Such cracks are produced by the pipe manufacturing process, because of the plastic deformations induced while bending the pipes to cope with the desired shape of the PV. In Table 1, computer tomography scan CT number 6078 is highlighted

(red) because it is the chosen specimen to simulate the fatigue crack propagation by FEM analysis.

In Figure 5, the special machine used for bending the welded pipe on the heat sink is shown. During the pipe bending, some cracks could be created within the seam. These cracks are arranged along the weld seam. The study proposed herein considers a set of these cracks as a single equivalent crack. This type of modelling is technically adequate to describe the problem of the fatigue crack propagation in a welded assembly.

The failure criterion adopted to stop the fatigue test is defined as the crack propagating through the pipe thickness that causes a fluid leakage. To automatically detect such a condition, an under pressure is created inside the pipe and monitored continuously with a manometer. In Figure 6, one of the tested specimens is shown that highlight the cracked weld seam. A strain gauge is used for monitoring the deformation process. The strain gauge
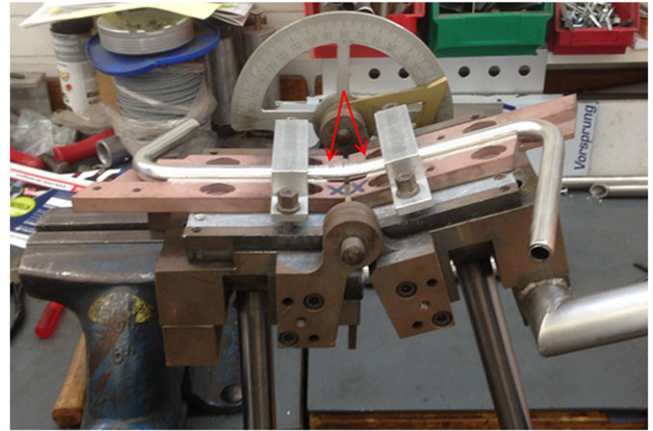
FIGURE 5 Pipe bending during the manufacturing process, highlighting the crack locations at the braze roots in between the two CuCrZr heat sinks (red arrows in the picture) [Colour figure can be viewed at wileyonlinelibrary.com]
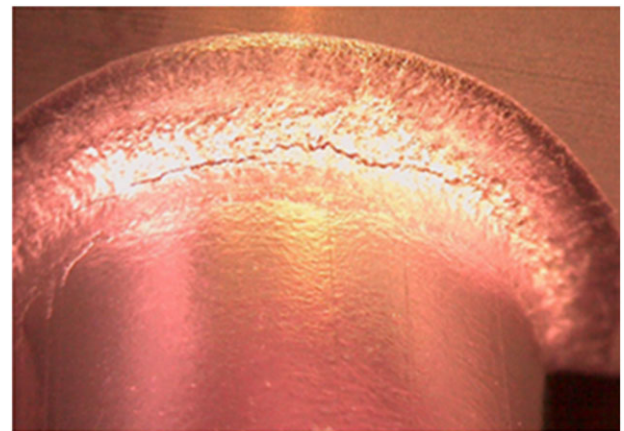
FIGURE 6 The root seam with highlighting of initial crack [Colour figure can be viewed at wileyonlinelibrary.com]

was introduced near the weld seam and was used for verifying the accuracy of the calibrated FE model for the fatigue crack propagation.

3.2 | Experimental fatigue test

Four fatigue tests were performed considering a maximum fatigue load of 1 kN (stress ratio $R = 0.1$, frequency f = 10 Hz): the related results are reported in Table 4. Only the P3 and P6 tests contain a crack both within the weld seam and the steel pipe, while the P4 and P1 tests contain a crack only in the weld seam. The results from these experimental tests are reported in Table 4. Among these results, the P3 test is highlighted in red to represent the numerically simulated test.

The simulation of the fatigue test of specimen P3 was performed using an FEM-based model, in which a spring of calibrated stiffness was introduced at the point of load application. Such a spring has been introduced to match the numerical and experimental results (Figure 7).

3.3 | FEM-based numerical test

The FEM-based model is related to a straight pipe, in the configuration preceding the plastic deformation of the specimen N. 6078 (Table 3). Subsequently, bending is simulated by an elastic plastic FEM analysis until the

TABLE 4 Fatigue test results

Probe	Braze Seam	Failure
P4	2i	No failure up to 60 000 cycles
P6	2a	Failure at 30 530 cycles
P3	**1i**	**Failure at 34 346 cycles**
P1	2i	No failure up to 60 000 cycles

final angle of 168° is reproduced. At the end of this phase, the residual stresses arising owing to such a preliminary pipe deformation are available for the subsequent load steps.

In Figure 8, the FEM-based model at crack insertion and at the end of the static test is shown. The FE model has been meshed using 152 430 linear elements with 175 120 nodes, plotted on the deformed scale, magnified 200×, and subsequently undeformed. This deformed model is required to demonstrate some details of the open crack more accurately.

In Figure 9, the crack surface between the braze seam and steel pipe is shown, highlighting only the cracked region. It is noteworthy that of the mixed mode I-II is obtained[1,4] and the plastic zone is small compared with the body dimensions such that the SSY conditions are still valid. The upper scale of the contour plot is equal to the yield stress to demonstrate the portion of the material surrounding the crack that exceeds the yield limit. This configuration is related to that of the crack insertion step. Initial crack has a shape clearly visible from observation of Figure 9. The crack is about 20 mm wide, and the deepest point along the crack front is at about 0.6 mm from the welding seam. The remaining ligament is approximately 0.76 mm in the steel pipe (see Figure 9). Other information about techniques employed to model initial crack can be found in the literature.[13,21-23]

After 34 837 cycles of fatigue crack propagation, the part of material surrounding the crack that exceeds the yield limit is increased but insufficient to produce material breakage for plastic collapse. It is noteworthy that, in this calculation, only linear elements were used. Thus, this result could have poor accuracy. This is the case shown in Figure 10, in which some elements of the mesh on the inner surface of the pipe exceed the yield stress. However, at approximately this level of cycle fatigue, the leakage phenomenon was observed experimentally.
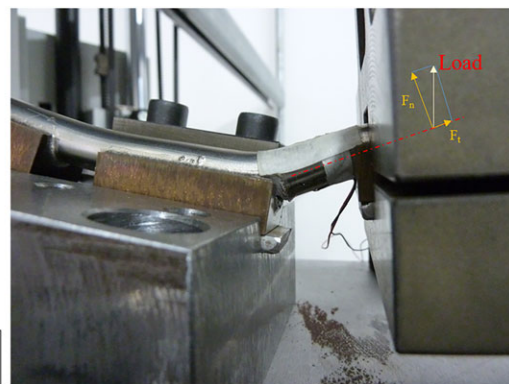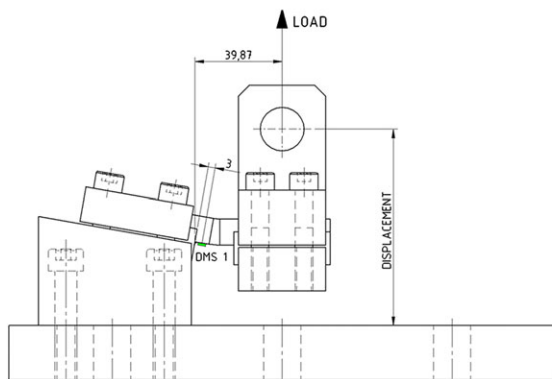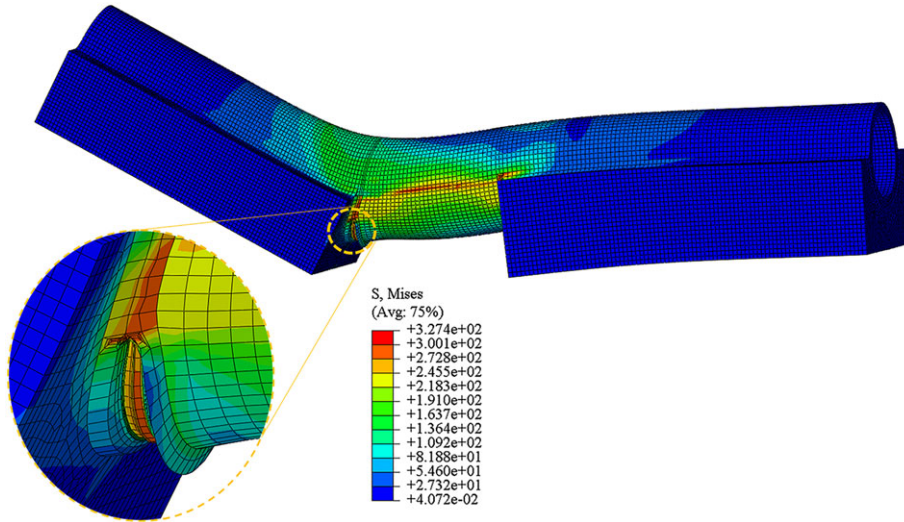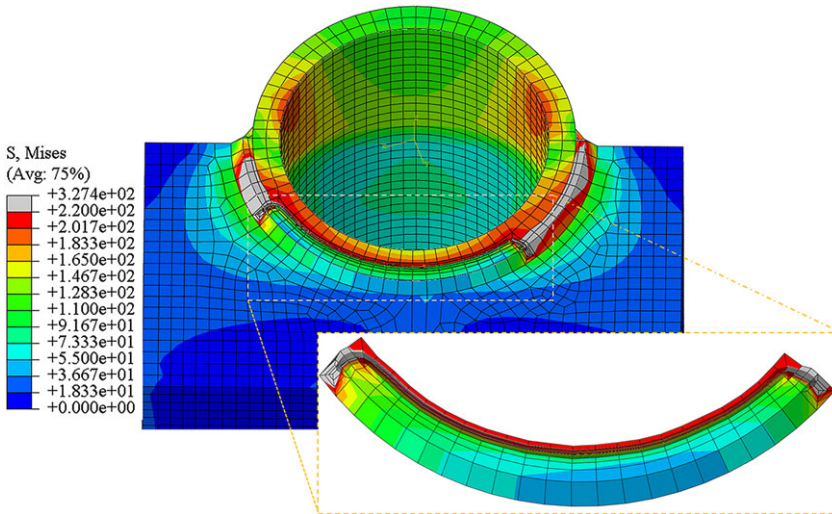

FIGURE 7 Direction of the applied load is not maintained orthogonal to the pipe axis during the test [Colour figure can be viewed at wileyonlinelibrary.com]

FIGURE 8 FE model at the end of the static test (third step) [Colour figure can be viewed at wileyonlinelibrary.com]

FIGURE 9 Small yielding occurs along the crack front. The upper scale of the von Mises stresses is equal to 220 MPa (yield stress) [Colour figure can be viewed at wileyonlinelibrary.com]
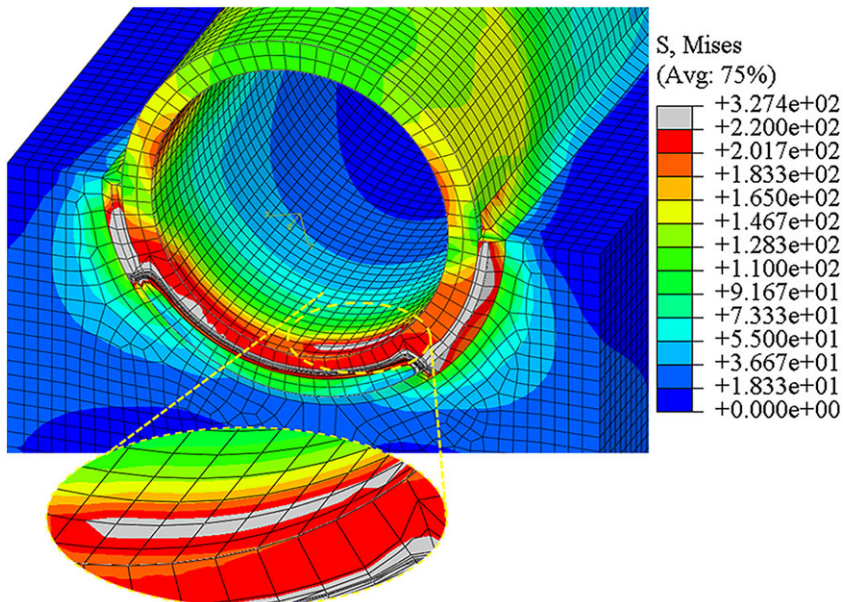
FIGURE 10 Cracked zone at 34 837 cycles of fatigue propagation highlighting the inner surface of the pipe in which the yield limit is exceeded [Colour figure can be viewed at wileyonlinelibrary.com]

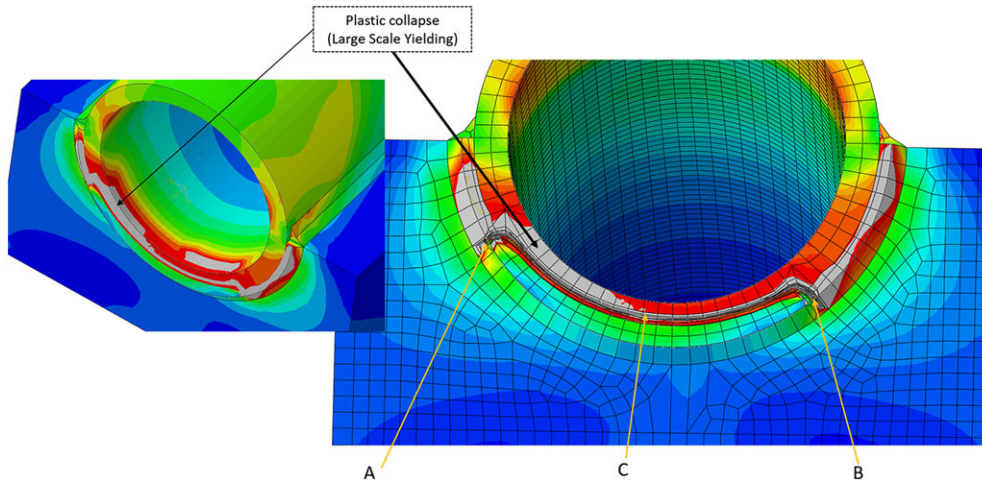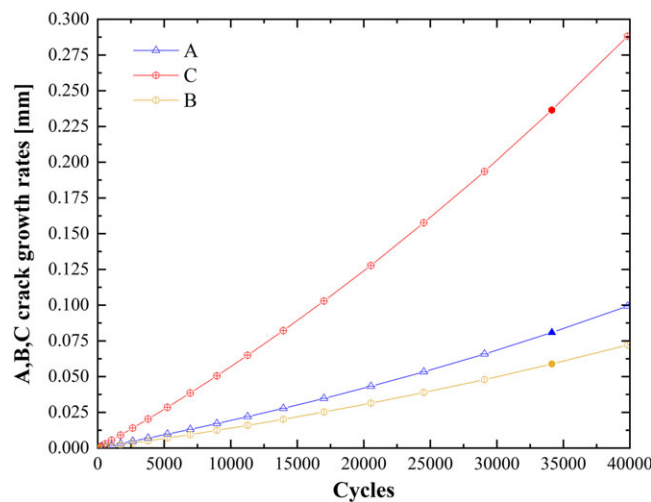**FIGURE 11** Cracked region highlighting the extended plasticisation. Furthermore, the regions of plastic collapse are clearly shown [Colour figure can be viewed at wileyonlinelibrary.com]

FIGURE 12 Increments of the crack front points A,B,C vs number of cycles [Colour figure can be viewed at wileyonlinelibrary.com]

Figure 10 shows the penultimate fatigue crack propagation step, namely the useful step to estimate the propagation life of the steel pipe. In Figure 11, the last step of the fatigue crack propagation is shown. The yield limit is exceeded in a large braze seam and steel pipe, for which SSY cannot be considered as more valid. The cracked region affected by a large plasticisation belongs to the LSY condition. At this level of plasticity, the leakage phenomenon is remarked experimentally. The number of end-of-cycles is therefore estimated at 39 830 cycles of fatigue crack propagation.

3.4 | Numerical crack growth rates

In Figure 12, the overall crack growth rates are reported. The expected propagation life corresponds to 34 346 cycles of fatigue crack propagation, namely when the leakage phenomenon occurs. In the numerical analysis of fatigue crack propagation, both LSY and plastic collapse occur at this step of crack propagation. Three measuring points were considered to plot the crack growth rates, namely A, B, and C. The A and B points correspond to the surface break-through point, while C is the middle position break-through point. This latest configuration of the crack appears comparable with the postmortem investigation performed with X-ray from the BAM centre in Berlin.

4 | CONCLUSIONS

In this study, a crack of considerable size was initially inserted both into the braze seam and into the pipe of the baffle module of Wendelstein 7-X. Further, it was maintained closed using the CCFT. During the

simulation of the pipe bend test, the constraint previously imposed on the crack faces was removed, allowing the crack to open and redistribute the residual stresses, thus causing the body to reach a new equilibrium.

Subsequently, the crack was modelled to be comparable to one of the real cracks measured by scan tomography on the affected components. Additionally, an FEM-based cracked model was used to simulate a pure bending test. Furthermore, in the FE model, a calibrated spring was introduced in the Z-direction to reproduce the behaviour of the experimental test. Hence, a two-scale model for fatigue crack propagation in SSY conditions was adopted to assess the fatigue crack propagation of the specimen until plastic collapse occurred, similar to the experimental tests.

The crack growth rates obtained at the end of the numerical simulation showed a satisfactory agreement with the experimental results. In fact, the numerical analysis indicated that the leakage of the specimen probably occurred between 34 137 and 39 830 cycles of fatigue crack propagation very close to the experimental value of 34 346 cycles.

ORCID

Marcello Lepore https://orcid.org/0000-0001-6065-1866
Filippo Berto https://orcid.org/0000-0001-9676-9970

REFERENCES

1. Aliha MRM, Bahmani A, Akhondi S. Numerical analysis of a new mixed mode I/III fracture test specimen. *Eng Fract Mech*. 2015;134:95-110.

2. Aliha MRM, Berto F, Bahmani A, Gallo P. Mixed mode I/II fracture investigation of Perspex based on the averaged strain energy density criterion. *Phys Mesomech*. 2017;20(2):149-156.

3. Berto F, Gomez G. Notched plates in mixed mode loading (I+II): a review based on the local strain energy density and the cohesive zone mode. *Eng Solid Mech*. 2017;5(1):1-8.

4. Berto F, Lazzarin P, Kotousov A, Pook LP. Induced out-of-plane mode at the tip of blunt lateral notches and holes under in-plane shear loading. *Fatigue Fract Eng Mater Struct*. 2012;35(6):538-555.

5. Brocks W. *Plasticity and Fracture. Solid Mechanics and Its Applications*. 244. Berlin Germany: Springer; 2018.

6. Cherepanov CP. Crack propagation in continuous media. *Appl Math Mech*. 1967;31:476-488.

7. Citarella R, Giannella V, Lepore MA, Fellinger J. FEM-DBEM approach to analyse crack scenarios in a baffle cooling pipe undergoing heat flux from the plasma. *AIMS Mater Sci*. 2017;4(2):391-412.

8. Citarella R, Lepore M, Fellinger J, Bykov V, Schauer F. Coupled FEM-DBEM method to assess crack growth in magnet system of Wendelstein 7-X. *Frattura ed Integrita Strutturale*. 2013;26:92-103.

9. Citarella R, Lepore M, Perrella M, Fellinger J. Coupled FEM–DBEM approach on multiple crack growth in cryogenic magnet system of nuclear fusion experiment 'Wendelstein 7-X'. *Fatigue Fract Eng Mater Struct*. 2016;39(12):1488-1502.

10. DeLorenzi H.G. Energy release rate calculations by the finite element method. General Electric Technical Information Series, Report No. 82CRD205, 1982.

11. DeLorenzi HG. On the energy release rate and the J-integral for 3D crack configurations. *J Fracture*. 1982;19(3):183-193.

12. Edmunds TM, Willis JR. Matched asymptotic expansions in non-linear fracture mechanics-iii. In-plane loading of an elastic perfectly plastic symmetric specimen. *J Mech Phys Solids*. 1977;25(6):423-455.

13. Fellinger J, Citarella R, Giannella V, et al. Overview of fatigue life assessment of baffles in Wendelstein 7-X. *Fusion Eng Des*. 2018;136:292-297.

14. Franc3D v7.2 – 2018. Documentation. Fracture Analysis Consultants, Inc.

15. Giannella V, Citarella R, Fellinger J, Esposito R. LCF assessment on heat shield components of nuclear fusion experiment "Wendelstein 7-X" by critical plane criteria. *Procedia Struct Integr*. 2018;8:318-331.

16. Hilton PD, Hutchinson JW. Plastic intensity factors for cracked plates. *Eng Fract Mech*. 1971;3(4):435-451.

17. Huffman PJ. A strain energy based damage model for fatigue crack initiation and growth. *Int J Fatigue*. 2016;88:197-204.

18. Hutchinson JW. Crack-tip singularity fields in non-linear fracture mechanics: a survey of current status. *Adv Fract Res*. 1982;6:2669-2684.

19. Kujawski D, Ellyin F. A fatigue crack growth model with load ratio effects. *Eng Fract Mech*. 1987;28(4):367-378.

20. Kuna M. *Finite Elements in Fracture Mechanics. Solid Mechanics and Its Applications*. 201. Berlin Germany: Springer; 2013.

21. Lepore M, Berto F. On the fatigue propagation of multiple cracks in friction stir weldments using linear and non-linear models under cyclic tensile loading. *Eng Fract Mech*. 2019;206:463-484.

22. Lepore M, Berto F, Kujawski D. Non-linear models for assessing the fatigue crack behaviour under cyclic biaxial loading in a cruciform specimen. *Theor Appl Fract Mech*. 2019;100:14-26.

23. Lepore M, Carlone P, Berto F, Sonne MR. A FEM based methodology to simulate multiple crack propagation in friction stir welds. *Eng Fract Mech*. 2017;184:154-167.

24. Li FZ, Shi CF, Needleman A. A comparison of methods for calculating energy release rates. *Eng Fract Mech*. 1985;21(2):405-421.

25. Noroozi AH, Glinka G, Lambert S. A two parameter driving force for fatigue crack growth analysis. *Int J Fatigue*. 2005;27(10-12):1277-1296.

26. Noroozi AH, Glinka G, Lambert S. A study of the stress ratio effects on fatigue crack growth using the unified two-parameter fatigue crack growth driving force. *Int J Fatigue*. 2007;29(9-11):1616-1633.

27. Parks DM. A stiffness derivative finite element technique for determination of crack tip stress intensity factors. *Int J Fract.* 1974;10(4):487-502.

28. Parks DM. The virtual crack extension method for non-linear material behaviour. *Comput Methods Appl Mech Eng.* 1977;1:353-364.

29. Portella P.D., Rie K.-T. Low Cycle Fatigue and Elasto-Plastic Behaviour of Materials. 1998. Pag. 530.

30. Razavi SMJ, Aliha MRM, Berto F. Application of an average strain energy density criterion to obtain the mixed mode fracture load of granite rock tested with the cracked asymmetric four-point bend specimens. *Theor Appl Fract Mech.* 2018;97:419-425.

31. Rice JR. A path independent integral and the approximate analysis of strain concentrations by notches and cracks. *J Appl Mech.* 1968;35(2):379-386.

32. Wolf RC, Ali A, Alonso A, et al. Major results from the first plasma campaign of the Wendelstein 7-X stellarator. *AIEA Nuclear Fusion.* 2017;57(10):1-13.

33. Zehnder AT. *Fracture Mechanics. Lecture Notes in Applied and Computational Mechanics.* 62. Berlin Germany: Springer; 2012.

34. Zencrack v8.3.1–2018. Documentation. Zentech International Limited.